Metallomics

PAPER



Cite this: *Metallomics*, 2020, **12**, 1000

# A liver-targeting Cu(I) chelator relocates Cu in hepatocytes and promotes Cu excretion in a murine model of Wilson's disease†

Marie Monestier,[ab] Anaïs M. Pujol,[ab] Aline Lamboux,[c] Martine Cuillel,[a] Isabelle Pignot-Paintrand,[d] Doris Cassio,[e] Peggy Charbonnier,[a] Khémary Um,[a] Amélie Harel,[a] Sylvain Bohic,[f] Christelle Gateau,[b] Vincent Balter,[c] Virginie Brun,[g] Pascale Delangle *[b] and Elisabeth Mintz*[a]

Received 18th March 2020,
Accepted 5th May 2020

DOI: 10.1039/d0mt00069h

rsc.li/metallomics

Copper chelation is the most commonly used therapeutic strategy nowadays to treat Wilson's disease, a genetic disorder primarily inducing a pathological accumulation of Cu in the liver. The mechanism of action of Chel2, a liver-targeting Cu(I) chelator known to promote intracellular Cu chelation, was studied in hepatic cells that reconstitute polarized epithelia with functional bile canaliculi, reminiscent of the excretion pathway in the liver. The interplay between Chel2 and Cu localization in these cells was demonstrated through confocal microscopy using a fluorescent derivative and nano X-ray fluorescence. The Cu(I) bound chelator was found in vesicles potentially excreted in the canaliculi. Moreover, injection of Chel2 either intravenously or subcutaneously to a murine model of Wilson's disease increased excretion of Cu in the faeces, confirming *in vivo* biliary excretion. Therefore, Chel2 turns out to be a possible means to collect and excrete hepatic Cu in the faeces, hence restoring the physiological pathway.

**Significance to metallomics**

Ionic copper (Cu) is both essential and toxic for any living organism. Vertebrates get rid of excess copper in their liver by transferring it from hepatocytes to the bile. Wilson's disease (WD) is a genetic disorder impairing this mechanism, thus leading patients to lifelong Cu chelation treatments. Because Cu primarily accumulates in the liver, we designed an hepatocyte-targeting molecule embedding a high affinity Cu(I)–chelator that is released in hepatocytes. Here, we elucidate the mechanism of action of this molecule at the cellular level and confirm that the liver-targeting chelator restores Cu excretion into the bile in WD mice.

## Introduction

A possible involvement of metal ions has been brought to the forefront in many neurodegenerative diseases without knowing whether the abnormal presence of metal ions is the cause or a consequence of the disease, for instance in Alzheimer's disease.[1] In some cases however, when the homeostasis of an essential metal ion is disrupted by a genetic defect, the excess of the given metal is known to be responsible for the disease; this is the case for iron in hemochromatosis and aceruloplasminemia, manganese in hypermanganesemia or copper in Wilson's disease.[2] Systemic metal chelation is the usual therapy for most of these diseases, in order to lower the dietary absorption of the metal ions and, hopefully, to deplete the excess stores by excreting the metal ions, often in urine. One striking observation is that these diseases promote a high increase in the liver content of the metal with disrupted homeostasis. Some metal ions also promote neurological symptoms with abnormal magnetic resonance images of the brain.[3]

Wilson's disease is an autosomal recessive disease resulting from mutations of the *ATP7B* gene, whose product is a Cu(I)-transporting ATPase, a membrane protein that pumps copper

[a] *Univ. Grenoble Alpes, CEA, CNRS, IRIG, LCBM, F-38000 Grenoble, France*
[b] *Univ. Grenoble Alpes, CEA, CNRS, IRIG, SyMMES, F-38000 Grenoble, France. E-mail: pascale.delangle@cea.fr*
[c] *Univ. Lyon, CNRS, ENS de Lyon, LGLTPE, F-69007 Lyon, France*
[d] *Univ. Grenoble Alpes, CNRS, Grenoble INP, LMGP, F-38000 Grenoble, France*
[e] *INSERM, Univ. Paris Sud, UMR U 1174, F-91405 Orsay, France*
[f] *Inserm, UA7, Synchrotron Radiation for Biomedicine (STROBE), 38000, Grenoble, France*
[g] *Univ. Grenoble Alpes, CEA, INSERM, IRIG, BGE, F-38000 Grenoble, France*

† Electronic supplementary information (ESI) available: Detailed experimental section. Supplementary fluorescence images (Fig. S1–S3), nano XRF images (Fig. S4 and S5). Supplementary data for the $^{65}$Cu experiments on mice (Fig. S6 and Table S1, S2)]. See DOI: 10.1039/d0mt00069h

out of the cytoplasm. Under normal conditions, the so-called Wilson protein is in the *trans*-Golgi network for dispensing copper to enzymes that use it as a co-factor. In case of excess copper in the cell, the Wilson protein changes its localization for pumping copper into intracellular vesicles that will eventually excrete it out of the cells.[4] The *ATP7B* gene is expressed mainly in the liver and the brain and to a lesser extent in kidney, lung, placenta, mammary gland and intestine.[4,5] Because vertebrates get rid of the excess copper by transferring it into the bile and then the faeces, the Wilson protein is responsible for the detoxification of the whole organism. Therefore, mutations in *ATP7B* gene primarily induce a pathological accumulation of copper in the liver.[6,7] Over the years, the liver undergoes fibrosis, cirrhosis and in some cases, acute hepatitis that requires a liver transplantation for the patient to survive. In addition, about 40% of the Wilson's disease patients develop neurological symptoms and 20%, psychiatric symptoms with no obvious signs of chronic liver disease. Among the patients with a neurological presentation, those who underwent a liver transplantation generally improved their condition. Their liver was loaded with copper, even though these patients did not necessarily exhibit typical signs of a liver condition.[8–10]

The heterogeneous clinical presentations and the late onset of the neurological signs make Wilson's disease difficult to diagnose from scratch, even though there is a clear MRI signature in the brain and many patients have a large copper overload at the time of diagnosis. The chelators prescribed all over the world are D-penicillamine and triethylenetetramine, two molecules that allow some copper removal of the body. Unfortunately, they also have adverse effects which preclude their use, in up to 30% of the patients in the case of D-penicillamine.[11] One major drawback of these molecules is that they are systemic and used at high dosage. They are only moderately specific for the excess copper stored in hepatocytes, especially when one has in mind the very high affinity and specificity found in proteins devoted to copper homeostasis.[12]

Given these observations, we have developed in the past decade bio-inspired chelators mimicking the Cu(I) binding sites from two cysteine-rich proteins involved in copper homeostasis.[12,13] One chelator mimics a metallochaperone binding site with a $CuS_2$ coordination[14] and the other one mimics a metallothionein binding site with a $CuS_3$ coordination.[15,16] To protect the Cu(I) binding sites until they reach their target, the chelator's thiol functions have been oxidized into disulphide bonds, so that Cu(I) chelation would be activated only once inside the cells. Indeed, intracellular glutathione is millimolar and ensures the reduction of the disulphide bonds.[14,17] Finally, because Wilson's disease starts in the hepatocytes, the so-designed pro-chelators were grafted with ligands that specifically recognize the asialoglycoprotein receptors (ASGPR) at the hepatocyte sinusoidal membrane.[18] The design and the efficiency of the final molecules, *i.e.* the hepatocyte targeting pro-chelators, have been described earlier.[19] These studies, performed on hepatocyte-derived cell lines, show that both ASGPR-targeting pro-chelators release an efficient Cu chelator inside the cells, suggesting these compounds were models for the development of new hepatocyte- and Cu(I)-specific

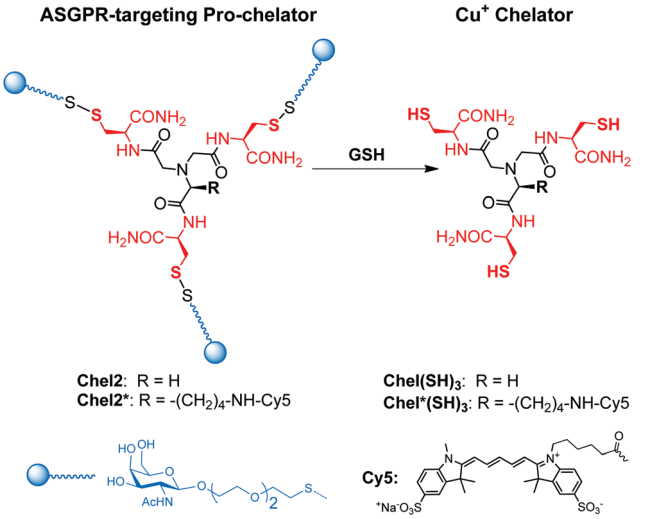


Scheme 1 Structures of the glycoconjugates Chel2 and Chel2* and the released chelators Chel(SH)$_3$ and Chel*(SH)$_3$.

chelators. However, the intracellular mechanism of action of the chelators and the fate of the Cu(I) chelator complexes are still to be determined.

The work reported here aims at understanding the mechanism of action of Chel2 (Scheme 1), the hepatocyte-directed pro-chelator releasing a tristhiolate chelator in the cells.[17]

We first studied Chel2 mechanism of action in WIF-B9 cells reconstituting a polarized epithelium. We report on the trafficking of Chel2*, a sulphocyanin5 labelled version of Chel2 and on the effects of Chel2 on the intracellular distribution of metal ions, following their X-ray fluorescence at the sub-micron scale (nano XRF) thanks to the ESRF synchrotron beam in Grenoble. Based on these studies, we propose a mechanism of action for the pro-chelator which would result in the transfer of the Cu(I)–chelator complex into the bile. This mechanism was further tested on *ATP7b*$^{-/-}$ mice, an animal model of Wilson's disease which develops the hepatic form of the disease.[20] To this end, *ATP7b*$^{-/-}$ mice were administrated $^{65}$Cu which accumulated in their liver. We found that a treatment with Chel2 increased the $^{65}$Cu content of the mice faeces, in agreement with partial restoration of the physiological pathway for Cu excretion through the bile.

## Results

Chel2 has been shown to release in WIF-B9 cells the high affinity Cu(I) chelator, Chel(SH)$_3$ (Scheme 1).[17] The latter is a tripodal sulphur chelator based on a nitrilotriacetic core grafted with three cysteine moieties that chelate Cu(I) with properties reminiscent of metallothioneins. The complex, denoted Chel$S_3$Cu, exhibits a $CuS_3$ coordination and an affinity constant as large as $10^{19}$.[16,21] In the hepatocyte-targeting pro-chelator Chel2, the three thiol functions are hidden in disulphide bridges carrying the targeting units, namely three polyethylene glycol chains grafted with *N*-acetyl galactosamine

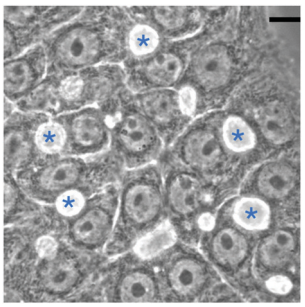

Fig. 1 Phase contrast image of living WIF-B9 cells forming bile canaliculi (phase lucent structures *), scale bar 10 μm.

moieties to get an architecture perfectly adapted for the interaction with the ASGPR.[19]

The hepatocyte-derived WIF-B9 cells are able to reconstitute remarkably stable and polarized epithelia with functional bile canaliculi, indicated by asterisks in Fig. 1.[22]

WIF-B9 cells provide a means to follow the detoxification function of the Wilson protein in case of excess copper. Indeed, the latter protein, localized at the *trans*-Golgi network membrane under normal conditions, migrates to the canalicular membrane in case of excess copper.[23] Hence, the localization of the Wilson protein, as detected by immunofluorescence, can be used to evaluate whether the intracellular Cu concentration is normal or in excess.[23] Under conditions where ATP7B co-localized with an apical membrane marker (*i.e.* the WIF-B9 canalicular membrane), addition of Chel2 into the culture medium actually suppressed the need for detoxification, as illustrated by the re-localization of ATP7B back to the *trans*-Golgi network.[14,17] These experiments demonstrate that the ASGPR-targeting pro-chelators are indeed doing what they were designed for, namely intracellular copper chelation. While performing these experiments, we found that 1 μM copper added to the WIF-B9 culture medium for 2 h is enough to induce the change in the ATP7B localization. Therefore, we could avoid the high concentrations used in previous studies on the localization of the ATP7B protein in WIF-B9 cells and other cell lines such as HepG2, HuH-7, CHO or HEK, where 20 to 200 μM Cu was used.[23–27] In the experiments reported hereafter, added Cu was either 1 or 15 μM. They were designed to study the localization of the Cu(I) chelator in hepatic cells and its effect on intracellular Cu distribution.

### Chel2* localization in WIF-B9 cells

Endogenous asialoglycoproteins such as asialo-ceruloplasmin, -fetuin or -orosomucoid, are known to be cleared from the circulation after binding to ASGPR,[28] a receptor of the hepatocyte sinusoidal membrane. In the rat liver, half a million ligand-binding sites per cell allow asialoglycoprotein–ASGPR complexes to undergo endocytosis.[29,30] Internalization is rapid (4–5 min at 37 °C)[31] and followed by a separation of ASGPR-containing vesicles that are found at the Golgi complex and ligand-containing vesicles that prefigure lysosomes.[32–34] The receptor is recycled by returning to the sinusoidal membrane, whereas the majority of the asialoglycoproteins is degraded in lysosomes. Yet, 1–4% of the asialoglycoproteins is kept intact and secreted into the bile across the canalicular membrane, a phenomenon called transcytosis that primarily depends on the protein.[31,35,36]

To get further insights into the fate of Chel2, we designed Chel2*, an analogue compound bearing a red fluorescent tag.[19] In Chel2* the sulphocyanin5 red fluorescent tag is tethered to the nitrilotriacetic acid scaffold through an amide bond.[19] When the disulphide bridges are cleaved by the reducing medium of the cell, namely glutathione, the red-fluorescent tag is still attached to the released chelator Chel*$(SH)_3$ (see Scheme 1). Because we do not know exactly at which stage the chelator is released, the red fluorescence in confocal microscopy was assigned either to the whole molecule (Chel2*), the free chelator Chel*$(SH)_3$ or to the copper–chelator complex Chel*$S_3Cu$, depending on the redox state of the molecule and the presence of Cu.

After 2 h of incubation with 1 μM Cu, 1 μM Chel2* was added to the culture medium for 30 min, 1 h or 2 h. Various compartments identified during endocytosis were marked by green fluorescence and co-localization was analysed on confocal laser scanning microscopy images, assigning a yellow colour to the co-localization pixels (Fig. 2). The images shown in Fig. 2 were chosen among about 40 images analysed for Che2* localization in various organelles. Additional images are shown in Fig. S1 in the ESI.† After 30 min (Fig. 2A), Chel2* was found in early endosomes (EEA1), close to the nuclei and in late endosomes or lysosomes (Lamp1), close to the bile canaliculi, but not in the *trans*-Golgi network (P58K). The latter finding confirms that Chel2* and ASGPR were segregated at that time.[37] There was still some co-localization with late endosomes after 1 h (Rab7, Fig. 2B), and with lysosomes/late endosomes after 2 h (LysoTracker™ and Lamp1, Fig. 2C).

A remarkable feature of Chel2* is that we did not observe a uniform distribution of red fluorescence in the cytosol. The red fluorescence always appeared as spots of about 200 nm, suggesting it was trapped in vesicles on the endocytosis/transcytosis pathway.

### Chel2* reaches bile canaliculi

At this point, special attention was paid to the search for Chel2* in the canaliculi after 30 min to 3 h. To this end, we looked for canaliculi surrounded by Chel2* and analysed the fluorescence intensity profile across these canaliculi. Some images obtained at 1 and 3 h are shown in Fig. 3, where the canaliculus is defined thanks to the interferential profile in panels B and D. Details of the analysis leading to Fig. 3 are shown in Fig. S2 and images of other canaliculi are shown in Fig. S3, in the ESI.† After 1 h incubation, Chel2* detected from the red fluorescence profile is found at the border of the canaliculus close to the cell apical membrane (Fig. 3A and B) and after 3 h incubation, Chel2* is found in the middle of the canaliculus (Fig. 3C and D). This shows Chel2 can be transferred to the canaliculus.

### Copper intracellular distribution by nano XRF

To get further insights into the fate of the chelator and the Cu(I)–chelator complexes, the WIF-B9 cells were analysed for

 

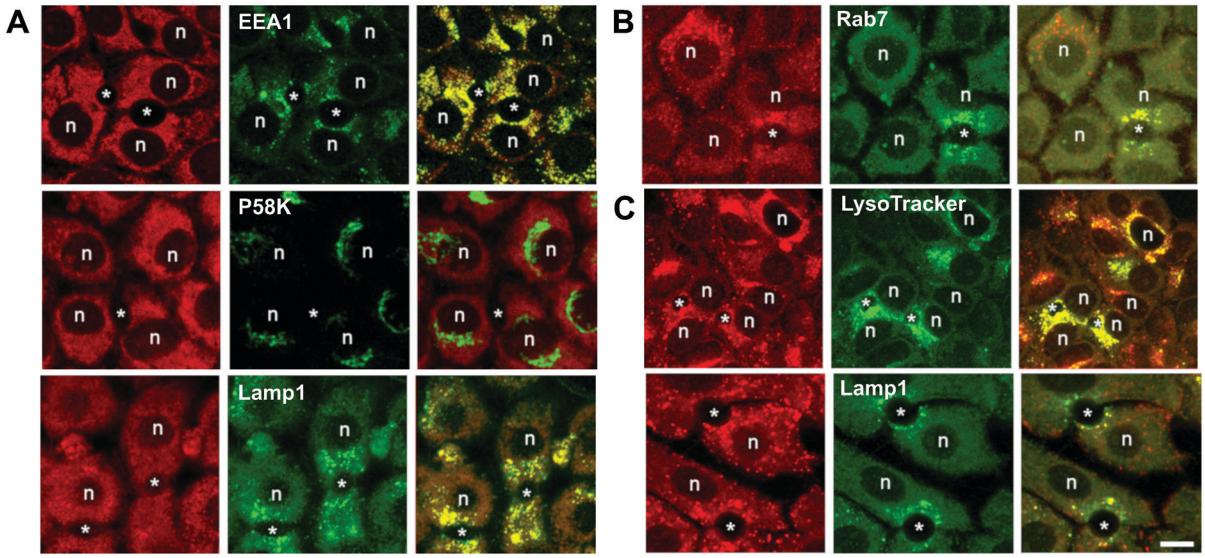


Fig. 2 Fluorescence images obtained by confocal microscopy of WIF-B9 epithelia forming canaliculi (*) and incubated for 2 h with 1 μM Cu and for (A) 30 min, (B) 1 h, (C) 2 h with 1 μM Chel2*. Left panels, red fluorescence of Chel2*; middle panels, green immunofluorescence of various protein markers or fluorescence of LysoTracker™ added 2 h before Chel2*; right panels, co-localization analysis, the yellow false colour is assigned to the co-localized pixels. EEA1: early endosomes, P58K: *trans*-Golgi network, LysoTracker™: lysosomes, Lamp1: late endosome/lysosome, Rab7: late endosomes. (n) nucleus, scale bar 10 μm.

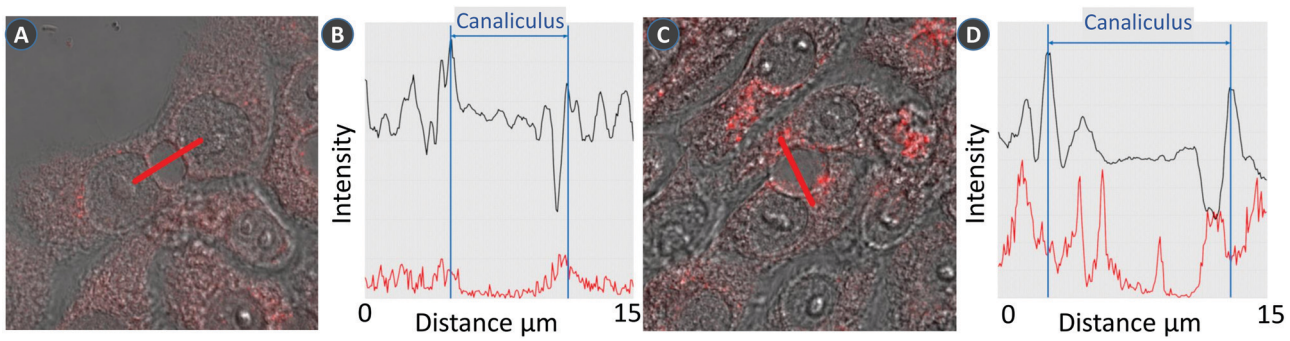


Fig. 3 Detailed analysis of Chel2* position in the region of the canaliculus. Analysis from interferential contrast and fluorescence images obtained by confocal microscopy of WIF-B9 epithelia forming canaliculi and incubated with 1 μM Chel2* for (A and B) 1 h or (C and D) 3 h. (A and C) merged images of interferential contrast and red fluorescence. The canaliculi are crossed by a 15 μm red line along which interferential contrast and fluorescence intensities are analysed. (B and D) interferential profiles in black and red fluorescence profiles along the line crossing the canaliculus.

their intracellular metal distribution, paying special attention to the bile canaliculi and the cytoplasmic region close to the canalicular membrane.

Nano XRF maps were performed on WIF-B9 cells forming a polarized epithelium and submitted to different conditions, starting with the basal culture medium, adding Cu for 2 h and then adding Chel2 for 3 h (Fig. 4). The nano XRF images shown in Fig. 4 are representative of the 2–5 canalicular regions scanned under each condition (Fig. S4 in the ESI†), bile canaliculi are indicated by asterisks. The P distribution covers the nuclei and the Zn distribution indicates the nuclei showing nucleoli as holes. Comparison with the phase image (Fig. 1) shows that the WIF-B9 organization and polarization were preserved by the sample preparation and the scans.

The image obtained under the basal conditions (Fig. 4A) shows two cells sharing a bile canaliculus and the Cu distribution is homogeneous across the cytoplasm with only scarce hot spots. After 2 h in the presence of 1 μM Cu, the Cu distribution shows a lot more hot spots in the three cells forming a canaliculus (Fig. 4B). Under the next condition, 5 h in 1 μM Cu including 50 μM Chel2 for the last 3 h, the Cu distribution appears concentrated along the apical membranes forming the canaliculus (Fig. 4C). All the scanned regions, whatever the condition, showed empty canaliculi, although their structure, and thus the cell organization, was preserved. The explanation for this observation was found by checking the distribution of abundant and loosely bound metal ions such as potassium or calcium. Actually, none of them was detectable, because the cryofixation step did permeabilize the cell membranes. Indeed, despite our efforts we did not succeed in finding a cryofixation method of WIF-B9 epithelia that would neither modify their membrane permeability nor break the canaliculi structure.

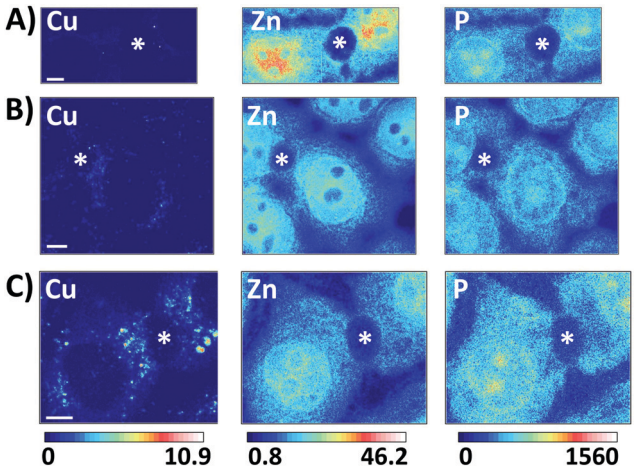


Fig. 4 Cell content analysed by nano XRF in WIF-B9 epithelia forming canaliculi under 3 different conditions: (A) basal conditions, (B) after 2 h with 1 μM Cu and (C) after 2 h with 1 μM Cu followed by addition of 50 μM Chel2 for 3 h. Under each condition, the Cu, Zn and P maps are shown. Scale bar 5 μm. The pixel size is 150 × 150 $nm^2$. Intensity scales are given in ng $cm^{-2}$.

The scans were next used to quantify the amount of Cu per surface unit. There was no significant change in whole scan Cu areal density (Fig. 5A) going from the basal conditions towards 1 μM Cu for 2 h; however, a clear-cut increase was observed in the presence of 15 μM Cu for 2 h ($P$ = 0.002). There was no further change in whole scan areal density when the cells were left for 3 more hours with 15 μM Cu. Some nano XRF images acquired with 15 μM Cu incubation are shown in Fig. S5 in the ESI.† These observations confirm that in the preparations, Cu homeostasis was active, the Wilson protein pumping Cu towards the bile canaliculus to protect the cell from extra Cu accumulation. A 50-fold excess of Chel2 in the presence of 1 μM Cu induced a significant increase in whole scan areal density of Cu when compared to the basal conditions ($P$ = 0.037). Bearing in mind that under these conditions, the Wilson protein is back at the *trans*-Golgi network as if the conditions were normal,[17] the extra Cu measured must be chelated or hidden from the intracellular medium. This shows that Chel2 has released the chelator in the cells ($Chel(SH)_3$, Scheme 1) and that the latter efficiently binds the excess Cu, becoming $ChelS_3Cu$ and thereby allowing more Cu to enter the cells from the culture medium.

The Cu areal density was also evaluated for regions of interest in the cells treated with 1 μM Cu, the nucleus and the canaliculus vicinity, denoted 'at bc' for 'surrounding the bile canaliculus'. The latter was defined as a crown around the canalicular membrane that was counted separately from the rest of the cytoplasm. The 'at bc' area accounts for 10.8 ± 1.1% of the cytoplasm area or 5.8 ± 0.4% of the whole scan area (mean ± SEM, $n$ = 16). Analysis of the Cu distribution in the cells (Fig. 5B) shows that only in the presence of Chel2, the 'at bc' area has an increased areal density, when compared to the basal condition ($P$ = 0.037). Interestingly, this demonstrates a Cu relocalization around the canaliculi upon Chel2 treatment.

### Faecal copper excretion in ATP7b$^{-/-}$ mice

Assuming that the relocalization of Cu seen in the nano XRF experiments reflects Cu excretion in the bile canaliculi due to Chel2 transcytosis, we next designed an experiment on *ATP7b*$^{-/-}$ mice to determine whether excess Cu could be found in their faeces after a treatment with Chel2. This section describes experiments performed on the *ATP7b*$^{-/-}$ mice kindly provided by Professor Svetlana Lutsenko.[20]

Tracing Cu excretion is feasible using Cu stable isotopes measured by multi-collector inductively coupled plasma mass spectrometry (MC-ICPMS). The MC-ICPMS technique gives access to natural variations of the $^{65}Cu/^{63}Cu$ ratio including biological samples such as cells, animal fluids and organs.[38–40]

Hence, we designed the following experiment. We reasoned that if the hepatic copper content could be enriched in $^{65}Cu$ by injecting a $^{65}Cu$ solution to the *Atp7b*$^{-/-}$ mice, we could collect their faeces during the following days and find out whether any $^{65}Cu$-enrichment could be measured. Assuming that Chel2 can

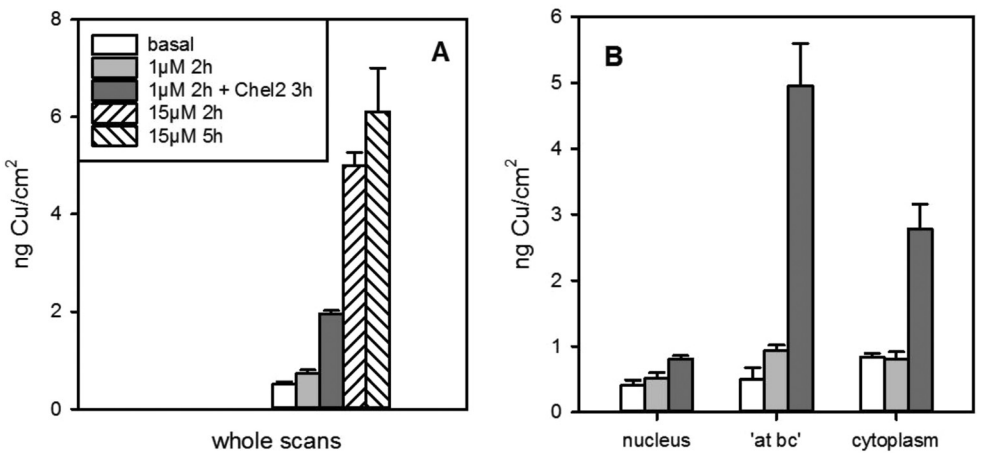


Fig. 5 Effects of Cu and Chel2 on the Cu areal density in WIF-B9 cells (mean and SE, standard error of the mean). In absence of Chel2, Cu was added to the culture medium at the concentration indicated in A. 50 μM Chel2 was added 2 h after Cu and left for 3 h. (A) Cu areal density of the whole scans; (B) Cu areal densities in the 3 subcellular regions, as indicated.

 

restore Cu excretion through the bile, *i.e.* the physiological pathway, then treating the mice by injecting Chel2 after the $^{65}$Cu injection should induce an increase in the $^{65}$Cu/$^{63}$Cu ratio in the faeces. We first evaluated how much excess $^{65}$Cu could be found in the liver from *Atp7b*$^{-/-}$ mice during the days following an intravenous (IV) injection of $^{65}$Cu. Preliminary experiments on 5 *Atp7b*$^{-/-}$ mice showed that after injecting ≈700 ng $^{65}$Cu, their liver contained ≈500 ng of excess $^{65}$Cu one or two days later. The 24 h-faeces collected in the meantime also contained excess $^{65}$Cu (11–22 ng g$^{-1}$ faeces) accounting for less than 5% of that found in the liver (487–660 ng g$^{-1}$ liver). Thanks to these results, we could envisaged to treat the mice with Chel2 for a week-long experiment.

Eight adult *Atp7b*$^{-/-}$ mice received an IV injection of 1–1.5 μg $^{65}$Cu at day −4 and from day 0 on, 8 IV injections of Chel2 (30 mg kg$^{-1}$, once a day for 4 days in a row, repeated the following week), as described in the upper panel of Fig. 6. The experiment was stopped on day 11. Another eight adult *Atp7b*$^{-/-}$ mice received Chel2 by subcutaneous (SC) injection instead of the IV route. The latter series lasted only one week and was stopped at day 4. Two other groups of 4 *Atp7b*$^{-/-}$mice were treated for control experiments that were stopped at day 4. They received either one dose of $^{65}$Cu at day −4 and 4 injections of buffer instead of Chel2, or one injection of vehicle at day −4 and 4 injections of Chel2. The faeces of all mice were collected every other day during treatment and at euthanasia, their liver was removed for analysis.

The excess of $^{65}$Cu, denoted $^{65}$Cu$_{xs}$ from now on, reflects in all samples the effect of the $^{65}$Cu spike on the isotopic Cu distribution. It is calculated by the difference between $^{65}$Cu$_{spl}$, the $^{65}$Cu amount measured in the sample and the natural $^{65}$Cu amount in the sample. The latter is calculated from $^{63}$Cu$_{spl}$, the $^{63}$Cu amount measured in the sample and $r_{ref}$, the natural $^{65}$Cu/$^{63}$Cu ratio measured in the isotopic standard NIST SRM 976 solution that always brackets the samples during the analysis.

Denoting $r_{ref}$ = $^{65}$Cu$_{ref}$/$^{63}$Cu$_{ref}$ and $r_{spl}$ = $^{65}$Cu$_{spl}$/$^{63}$Cu$_{spl}$, the isotopic ratio measured in the reference solution and the sample, respectively and designating by Cu$_t$ = $^{65}$Cu$_{spl}$ + $^{63}$Cu$_{spl}$, the total Cu measured in the sample, $^{65}$Cu$_{xs}$ is calculated as follows:

$$^{65}\mathrm{Cu}_{xs} = (r_{spl} - r_{ref}) \times {}^{63}\mathrm{Cu}_{spl},$$

$$\text{with } {}^{63}\mathrm{Cu}_{spl} \times (r_{spl} + 1) = \mathrm{Cu}_t,$$

$$\text{and finally } {}^{65}\mathrm{Cu}_{xs} = (r_{spl} - r_{ref})/(r_{spl} + 1) \times \mathrm{Cu}_t$$

The results are then expressed per unit of wet weight, ranging from 5 to 117 ng g$^{-1}$ for the faeces and from 0.1 to 1.4 μg g$^{-1}$ for the liver. In the control experiment where the mice did not receive $^{65}$Cu, the faeces collected after Chel2 treatment contained 0.2 ± 0.3 ng g$^{-1}$ excess $^{65}$Cu (mean ± SEM, $n$ = 8) and the 4 livers, −0.012 ± 0.001 μg g$^{-1}$ excess $^{65}$Cu (mean ± SEM, $n$ = 4), showing that r$_{spl}$ was not changed by the Chel2 treatment. In the other experiments where $^{65}$Cu was injected to the mice on day −4, dividing $^{65}$Cu$_{xs}$ obtained in the faeces by $^{65}$Cu$_{xs}$ obtained in the liver allows to evaluate $^{65}$Cu$_{xsF}$, the fraction of hepatic $^{65}$Cu excreted in the faeces, independently of individual variability. All the data is shown in Fig. 6 in permil.

Before any treatment, *i.e.* during the 24 h-period following the $^{65}$Cu injection, excess of $^{65}$Cu was evidenced in the faeces (see $^{65}$Cu$_{xsF}$ at day −3 in Fig. 6). In the mock group, where only the vehicle was injected for 4 days in a row, there was almost no more excess of $^{65}$Cu in each 24 h-faeces sample and $^{65}$Cu$_{xsF}$ value was around 15‰. Bearing in mind that these mice cannot excrete Cu from their liver, the measured $^{65}$Cu$_{xsF}$ value in the faeces at day −3 suggests the existence of an excretion pathway for Cu from blood to faeces, crossing the intestinal epithelium. The existence of such a Cu-excretion pathway has not been documented up to now. As a secondary excretion pathway appearing in the *Atp7b*$^{-/-}$ mice, it could also reflect the role of non-absorptive cells in the intestine.[41]

In the groups that received Chel2, either by IV- or by SC-injections, the fraction of hepatic $^{65}$Cu excreted in the faeces appeared higher than in the mock group. In a first attempt to interpret the effect of Chel2 on $^{65}$Cu$_{xsF}$, we pooled the data of each group on each day in Fig. S6 in the ESI,† which shows the mean and SEM ($n$ = 2 to 4). At first glance, the IV-treated mice excretion appeared stable for the two 4-day periods of treatment around 33‰, twice as much as the mock group (15‰). By contrast, the SC-treated animals excretion reached 45‰ at day 1 and tended to increase during the next days. Since we aimed at knowing whether Chel2 SC- or IV-treatment significantly increases the fraction of hepatic $^{65}$Cu excreted in the mice faeces, the data collected after treatment were pooled for each treatment and submitted to statistical analysis. The 3 groups were found statistically different by the nonparametric ANOVA

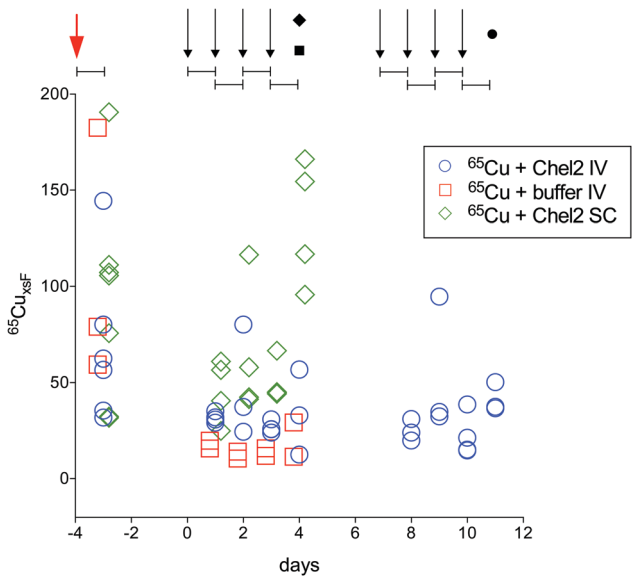


Fig. 6 Effect of Chel2 injections (starting at day 0, black arrows on top) on the fraction of hepatic $^{65}$Cu excreted in the faeces of mice ($^{65}$Cu$_{xsF}$ in permil) following an IV injection of $^{65}$Cu at day −4 (red arrow). (□) mock treatment: 4 mice received 4 IV injections of buffer from day 0 to day 4; (○) Chel2 IV-treatment: 7 mice received 8 IV injections of Chel2 (30 mg kg$^{-1}$) from day 0 to day 10; (◇) Chel2 SC-treatment: 8 mice received 4 SC injections of Chel2 (50 mg kg$^{-1}$) from day 0 to day 4. On top, segments figure the 24 h faeces collections and black symbols, euthanasia.

on ranks test. Pairwise comparisons show that both Chel2 treatments were statistically different from the mock treatment and that the SC-treatment was more efficient than the IV-treatment. All the data are listed in Table S1 and the statistical parameters are detailed in Table S2 in the ESI.† As a matter of fact, Chel2 is a highly hydrophilic compound, therefore expected to be rapidly cleared from the serum. Altogether, the IV injections were probably limiting the amount of Chel2 reaching the liver and crossing the hepatocytes. In contrast with the IV treatment, the SC injections were more effective in excreting excess $^{65}$Cu from the liver, suggesting a more progressive delivery of Chel2 to the liver.

## Discussion

The mechanism of action of Chel2, the liver-targeting Cu(I) chelator, was studied in WIF-B9 cells that reconstitute polarized epithelia with functional bile canaliculi. The relationship between Chel2 and Cu localization and distribution in these cells could be inferred from fluorescence confocal microscopy using the fluorescent derivative Chel2* and nano XRF, respectively.

For further discussion, we need to bear in mind that upon endocytosis in WIF-B9 cells, Chel2 releases Chel$(SH)_3$, the high affinity Cu(I) chelator. This was shown before, following the effect of Chel2 addition to the culture medium in the presence of 1 μM Cu on the Wilson protein localization and it provided the conditions used here for chelation (50 μM Chel2 + 1 μM Cu).[17] We can therefore expect the same for Chel2* (1 μM Chel2* + 1 μM Cu) which will also release the high affinity chelator. Therefore, we assign to Chel*$(SH)_3$ and Chel*$S_3$Cu(I) the red spots in Fig. 2 and 3.

Asialoglycoprotein endocytosis in polarized WIF-B9 cells has been previously studied and a remarkable feature is that the proteins pass through a subapical compartment that sorts them: some are sent to the lysosomes for degradation and others are sent to the apical membrane for transcytosis.[42] Using the same route with Chel2* instead of a protein, however, shows that there is co-localization with lysosomes and that red vesicles also concentrate around the canaliculi (Fig. 2). This suggests that after reduction of Chel2*, some Chel*$(SH)_3$ and Chel*$S_3$Cu are trapped in non-lysosomal vesicles on their way to exocytosis. Indeed, red fluorescence is seen in the middle of the canaliculus after 3 h (Fig. 3). Interestingly enough, these subapical vesicles could also be the hot spots of Cu seen by XRF, which would be full of Chel$S_3$Cu, under the chelation conditions (50 μM Chel2, Fig. 4C). Going back to the effect of 1 μM Cu for 2 h, we recall that under these conditions, ATP7B is found in the canalicular membrane, where it pumps Cu out of the cell, into the bile canaliculus.[17] According to Nyasae *et al.*[43] whose conclusions were derived from a similar polarized epithelium, we can assume ATP7B to have left the *trans*-Golgi network in vesicles and trafficked to the canalicular membrane *via* at first, basolateral endosomes and then, the subapical compartment. The same observation in Can-10 hepatic cells,[44] that are also able to reconstitute a polarized epithelium, suggests that in polarized hepatic cells, proteins undergoing transcytosis and proteins meant to reach the apical membrane

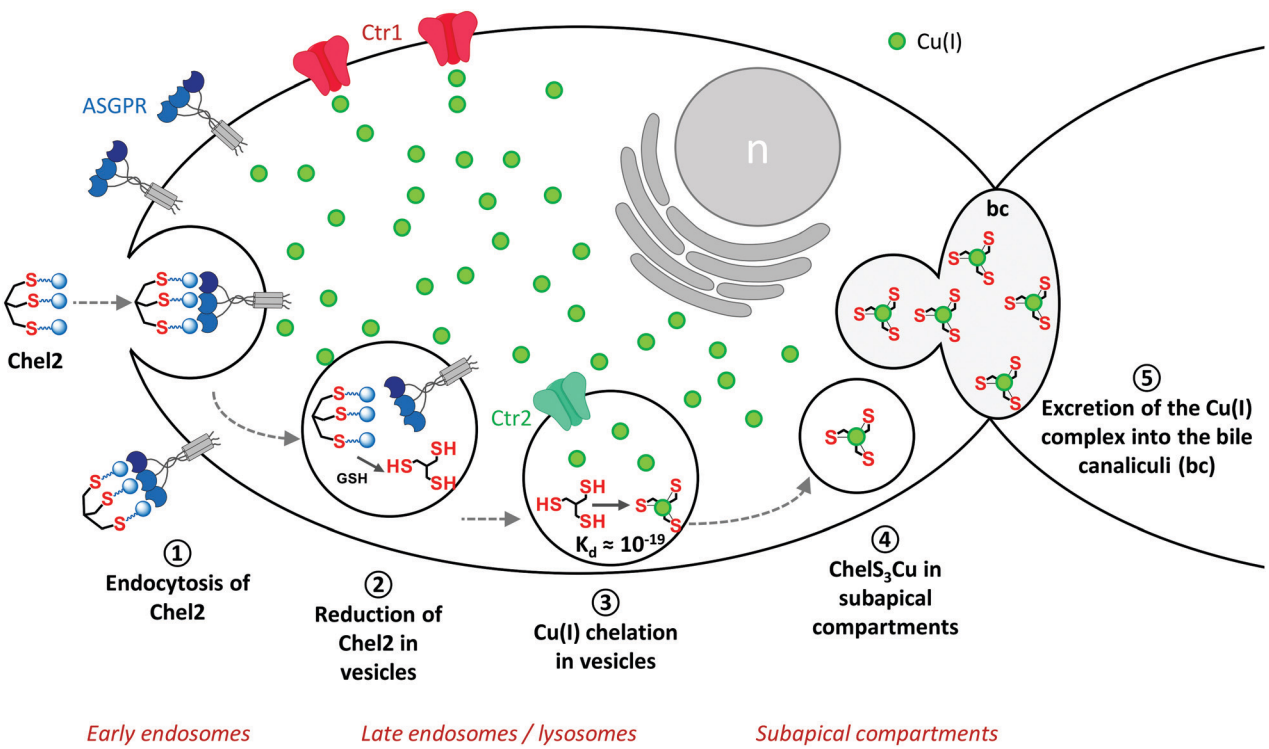


Scheme 2 Proposed mechanism for Chel2 fate in hepatic cells in the presence of Cu.

use the same route and there is no such a secretory pathway from the Golgi to the apical membrane. Therefore, we can assume that while being transported towards the canalicular membrane, ATP7B has pumped Cu inside the vesicles. Hence, the hot spots of Cu that are seen in the cytoplasm of the cells (Fig. 4B). In the presence of Chel2, endocytosis vesicles, that have a Cu transporter in their membrane,[45] are also able to accumulate Cu because Chel$(SH)_3$ binds Cu(I) inside the vesicles, hence creating a gradient for the Cu transporter. This will last until the normal ''free'' Cu concentration is reached, when ATP7B will return to the *trans*-Golgi network. At that time, the canalicular region will be full of subapical vesicles entrapping Chel$S_3$Cu and ready for exocytosis. All these observations led us to propose the mechanism shown in Scheme 2 for Chel2 fate in hepatic cells and its relationship with intracellular copper chelation. It can be described as follows: ① Chel2 binds to ASGPR and enters the hepatocytes by basolateral or sinusoidal endocytosis, ② Chel$(SH)_3$, the high affinity chelator, is released from Chel2 by reduction with GSH in these vesicles, ③ Chel$S_3$Cu, the Cu(I) complex, is formed in sinusoidal endocytic vesicles, ④ some vesicles fuse with lysosomes, while others become the subapical compartment and ⑤ the latter spills its load into the canalicular lumen leading to Cu excretion into the bile canaliculi.

If this were the mechanism occurring in *ATP7b*$^{-/-}$ hepatocytes, then Chel2 would restore the pathway for Cu excretion out of the liver. Our study with *ATP7b*$^{-/-}$ mice following excess $^{65}$Cu by MC-ICPMS supports this mechanism. Mice that received $^{65}$Cu followed by Chel2 treatment showed a significant increase of the $^{65}$Cu content in their faeces. This demonstrates increased Cu excretion after IV injections and even more efficiently after SC injections of Chel2 and most importantly excretion through the bile.

## Conclusions

In search of the mechanism of action of Chel2, the liver-targeting Cu(I) chelator, we observed in hepatocytes that among the Chel2 molecules that entered by endocytosis, some were localized in the lysosomes, whereas others were found in vesicles close to the canaliculus membrane, most probably in subapical compartments, and finally in the canaliculus lumen. Interestingly enough, hot spots of Cu were found surrounding the canaliculi in WIF-B9 cells, demonstrating that the chelator-containing vesicles were full of Cu. Because in polarized WIF-B9 cells, subapical compartments are known to fuse with the apical membrane, we assumed that the chelator released by Chel2 was expelled in the canaliculus lumen together with Cu. Therefore, intracellular Cu chelation by the high affinity chelator released by Chel2 is expected to occur in vesicles along Chel2 transcytosis pathway, leading ultimately to Cu excretion into the bile canaliculi. Importantly, Chel2 injection either intravenously or subcutaneously to a murine model of Wilson's disease increased excretion of Cu in the faeces, confirming the biliary excretion mechanism at the animal level. As things stand now, Chel2 turns to a possible means to collect and excrete hepatic Cu in the faeces, hence restoring the physiological pathway. It would be interesting to check this on bigger animals whose condition can be monitored daily, to envisage the use of Chel2 for patients who do not tolerate the current treatments of Wilson's disease.

## Author contributions

EM and PD designed and supervised the work. MM, AP and CG synthesized the molecules. MC, IPP, PC and DC optimized the cell experiments. SB, PD and EM performed the experiment at ESRF and SB performed the data quantitative analyses. KU, AH and VBr performed the animal studies. AL and VBa performed the $^{65}$Cu MC-ICPMS analyses. The manuscript was written through contributions of all authors.

## Conflicts of interest

''There are no conflicts of interest to declare''.

## Acknowledgements

We thank Prof. Svetlana Lutsenko for providing the *ATP7b*$^{-/-}$ mice, Sandrine Miesch-Fremy for technical support with the experiments on mice, Dr Michel Ferrand for fruitful discussions on the project and Dr Michaud-Soret for critical reading of the manuscript. We acknowledge ESRF committees for providing synchrotron radiation beamtime (proposal MD-714) and all the ID22-NI beamline staff for help during the experiment. This research was supported by the French National Agency for Research in the framework of the ''Investissements d'avenir'' Program (ANR-15-IDEX-02), the Labex ARCANE (ANR-11-LABX-003), the CBH-EUR-GS (ANR-17-EURE-0003) and the grant ''COPDETOX'' (ANR-11-EMMA-025), the ''Fondation pour la Recherche Médicale'' (grant DCM20111223043), the ''Programme transversal du CEA Technologies pour la santé'' (WILCOP) and ADDMEDICA, the company that funded the experiments with $^{65}$Cu on mice.

## Notes and references

1 D. Strausak, J. F. Mercer, H. H. Dieter, W. Stremmel and G. Multhaup, *Brain Res. Bull.*, 2001, **55**, 175.

2 A. Piperno, F. Bertola and A. Bentivegna, (2005, Feb 17) [Updated 2020 Jan 9]. Juvenile Hemochromatosis [Web page]. Barton, J.C.; Edwards, C.Q. (2000, Apr 3) [Updated 2018 Dec 6]. HFE Hemochromatosis [Web page]. De Gobbi, M.; Roetto, A. (2005, Aug 29) [Updated 2018 Feb 15]. TFR2-Related Hereditary Hemochromatosis [Web page]. Miyajima, H.; Hosoi, Y. (2003, Aug 12) [Updated 2018 Sep 27]. Aceruloplasminemia [Web page]. Tuschl, K.; Clayton, P.T.; Gospe, S.M. Jr *et al.* (2012, Aug 30) [Updated 2017 Feb 9]. Dystonia/Parkinsonism, Hypermanganesemia, Polycythemia and Chronic Liver Disease [Web page]. Weiss, K.H. (1999, Oct 22)

[Updated 2016 Jul 29]. Wilson Disease [Web page]. All retrieved February 9, 2020 from https://www.ncbi.nlm.nih.gov/books/NBK1116/.
3 F. Woimant and J. M. Trocello, *Handb. Clin. Neurol.*, 2014, **120**, 851.
4 S. Lutsenko, N. L. Barnes, M. Y. Bartee and O. Y. Dmitriev, *Physiol. Rev.*, 2007, **87**, 1011.
5 K. H. Weiss, J. Wurz, D. Gotthardt, U. Merle, W. Stremmel and J. Fullekrug, *J. Anat.*, 2008, **213**, 232.
6 J. M. Walshe, *Mov. Disord*, 2006, **21**, 142.
7 J. M. Walshe, *Mov. Disord*, 2007, **22**, 2216.
8 A. Stracciari, A. Tempestini, A. Borghi and M. Guarino, *Arch. Neurol.*, 2000, **57**, 384.
9 O. Guillaud, J. Dumortier, R. Sobesky, D. Debray, P. Wolf, C. Vanlemmens, F. Durand, Y. Calmus, C. Duvoux, S. Dharancy, N. Kamar, K. Boudjema, P. H. Bernard, G. P. Pageaux, E. Salame, J. Gugenheim, A. Lachaux, D. Habes, S. Radenne, J. Hardwigsen, O. Chazouilleres, J. M. Trocello, F. Woimant, P. Ichai, S. Branchereau, O. Soubrane, D. Castaing, E. Jacquemin, D. Samuel and J. C. Duclos-Vallee, *J. Hepatol.*, 2014, **60**, 579.
10 C. Laurencin, A. S. Brunet, J. Dumortier, L. Lion-Francois, S. Thobois, J. Y. Mabrut, R. Dubois, F. Woimant, A. Poujois, O. Guillaud, A. Lachaux and E. Broussolle, *Eur. Neurol.*, 2017, **77**, 5.
11 K. H. Weiss, F. Thurik, D. N. Gotthardt, M. Schafer, U. Teufel, F. Wiegand, U. Merle, D. Ferenci-Foerster, A. Maieron, R. Stauber, H. Zoller, H. H. Schmidt, U. Reuner, H. Hefter, J. M. Trocello, R. H. Houwen, P. Ferenci, W. Stremmel and E. Consortium, *Clin. Gastroenterol. Hepatol.*, 2013, **11**, 1028.
12 P. Delangle and E. Mintz, *Dalton Trans.*, 2012, **41**, 6359.
13 C. Gateau, E. Mintz and P. Delangle, in *Ligand Design in Medicinal Inorganic Chemistry* ed. T. Storr, Wiley-Blackwell, 2014, p. 287.
14 A. M. Pujol, M. Cuillel, O. Renaudet, C. Lebrun, P. Charbonnier, D. Cassio, C. Gateau, P. Dumy, E. Mintz and P. Delangle, *J. Am. Chem. Soc.*, 2011, **133**, 286.
15 A. M. Pujol, C. Gateau, C. Lebrun and P. Delangle, *J. Am. Chem. Soc.*, 2009, **131**, 6928.
16 A. M. Pujol, C. Gateau, C. Lebrun and P. Delangle, *Chem. – Eur. J.*, 2011, **17**, 4418.
17 A. M. Pujol, M. Cuillel, A.-S. Jullien, C. Lebrun, D. Cassio, E. Mintz, C. Gateau and P. Delangle, *Angew. Chem.*, 2012, **51**, 7445.
18 G. Ashwell and J. Harford, *Annu. Rev. Biochem.*, 1982, **51**, 531.
19 M. Monestier, P. Charbonnier, C. Gateau, M. Cuillel, F. Robert, C. Lebrun, E. Mintz, O. Renaudet and P. Delangle, *ChemBioChem*, 2016, **17**, 590.
20 O. I. Buiakova, J. Xu, S. Lutsenko, S. Zeitlin, K. Das, S. Das, B. M. Ross, C. Mekios, I. H. Scheinberg and T. C. Gilliam, *Hum. Mol. Genet.*, 1999, **8**, 1665.
21 A.-S. Jullien, C. Gateau, I. Kieffer, D. Testemale and P. Delangle, *Inorg. Chem.*, 2013, **52**, 9954.
22 C. Decaens, P. Rodriguez, C. Bouchaud and D. Cassio, *J. Cell Sci.*, 1996, **109**(Pt 6), 1623.
23 Y. Guo, L. Nyasae, L. T. Braiterman and A. L. Hubbard, *Am. J. Physiol.: Gastrointest. Liver Physiol.*, 2005, **289**, G904.
24 H. Roelofsen, H. Wolters, M. J. Van Luyn, N. Miura, F. Kuipers and R. J. Vonk, *Gastroenterology*, 2000, **119**, 782.
25 M. Harada, H. Kumemura, S. Sakisaka, S. Shishido, E. Taniguchi, T. Kawaguchi, S. Hanada, H. Koga, R. Kumashiro, T. Ueno, T. Suganuma, K. Furuta, M. Namba, T. Sugiyama and M. Sata, *Int. J. Mol. Med.*, 2003, **11**, 293.
26 D. Huster, M. Hoppert, S. Lutsenko, J. Zinke, C. Lehmann, J. Mossner, F. Berr and K. Caca, *Gastroenterology*, 2003, **124**, 335.
27 M. A. Cater, J. Forbes, S. La Fontaine, D. Cox and J. F. Mercer, *Biochem. J.*, 2004, **380**, 805.
28 H. J. Geuze, J. W. Slot, G. J. Strous, H. F. Lodish and A. L. Schwartz, *J. Cell Biol.*, 1982, **92**, 865.
29 G. Gregoriadis, A. G. Morell, I. Sternlieb and I. H. Scheinberg, *J. Biol. Chem.*, 1970, **245**, 5833.
30 P. A. Charlwood, E. Regoeczi and M. W. Hatton, *Biochim. Biophys. Acta*, 1979, **585**, 61.
31 H. Tolleshaug, *Int. J. Biochem.*, 1981, **13**, 45.
32 T. Tanabe, W. E. Pricer, Jr. and G. Ashwell, *J. Biol. Chem.*, 1979, **254**, 1038.
33 H. J. Geuze, J. W. Slot, G. J. Strous, H. F. Lodish and A. L. Schwartz, *Cell*, 1983, **32**, 277.
34 S. C. Mueller and A. L. Hubbard, *J. Cell Biol.*, 1986, **102**, 932.
35 P. Thomas and J. W. Summers, *Biochem. Biophys. Res. Commun.*, 1978, **80**, 335.
36 T. M. Chang and C. H. Chang, *Biochim. Biophys. Acta*, 1989, **1014**, 229.
37 P. P. Breitfeld, C. F. Simmons, Jr., G. J. Strous, H. J. Geuze and A. L. Schwartz, *Int. Rev. Cytol.*, 1985, **97**, 47.
38 V. Balter, A. N. da Costa, V. P. Bondanese, K. Jaouen, A. Lamboux, S. Sangrajrang, N. Vincent, F. Fourel, P. Telouk, M. Gigou, C. Lecuyer, P. Srivatanakul, C. Brechot, F. Albarede and P. Hainaut, *Proc. Natl. Acad. Sci. U. S. A.*, 2015, **112**, 982.
39 V. P. Bondanese, A. Lamboux, M. Simon, J. E. Lafont, E. Albalat, S. Pichat, J. M. Vanacker, P. Telouk, V. Balter, P. Oger and F. Albarede, *Metallomics*, 2016, **8**, 1177.
40 L. Sauzeat, E. Bernard, A. Perret-Liaudet, I. Quadrio, A. Vighetto, P. Krolak-Salmon, E. Broussolle, P. Leblanc and V. Balter, *iScience*, 2018, **6**, 264.
41 H. Pierson, H. J. Yang and S. Lutsenko, *Annu. Rev. Nutr.*, 2019, **39**, 75.
42 G. Ihrke, G. V. Martin, M. R. Shanks, M. Schrader, T. A. Schroer and A. L. Hubbard, *J. Cell Biol.*, 1998, **141**, 115.
43 L. K. Nyasae, M. J. Schell and A. L. Hubbard, *Traffic*, 2014, **15**, 1344.
44 V. Lalioti, R. Peiro, M. Perez-Berlanga, Y. Tsuchiya, A. Munoz, T. Villalba, C. Sanchez and I. V. Sandoval, *J. Cell Sci.*, 2016, **129**, 2190.
45 C. Y. Tsai, J. K. Liebig, I. F. Tsigelny and S. B. Howell, *Metallomics*, 2015, **7**, 1477.

 